

## Equilibrium and kinetic studies about sorption of uranium(VI) using the cross-linking chitosan submicron particles modified by ammonium fluotitanate

Zi Xin You, Yang Wang, Min Zhao, Jia Ying Zhang, Yong Heng Xing\*, Feng Ying Bai\*

College of Chemistry and Chemical Engineering, Liaoning Normal University, Dalian City 116029, China, emails: xingyongheng@lnnu.edu.cn (Y.H. Xing), baifengying2000@163.com (F.Y. Bai)

Received 9 February 2018; Accepted 5 July 2018

### ABSTRACT

The cross-linking chitosan submicron particles modified by ammonium fluotitanate (Ti/CTS) was obtained and used as a new low-cost adsorbent for radioactive uranyl ion from aqueous solutions. The prepared adsorbent was characterized by Fourier transform infrared spectroscopy, scanning electron microscope, Brunauer–Emmett–Teller, and X-ray diffraction. In addition, measurements and effects of the initial pH, contact time, adsorbent dosage, initial concentration of U(VI), and temperature on the adsorption of U(VI) ions were studied in detail. The results indicated that the Ti/CTS exhibited excellent adsorption properties. The maximum adsorption capacity of Ti/CTS was  $195 \text{ mg g}^{-1}$ . It was found that the adsorption equilibrium data could be best fitted to the pseudo-second-order model. In the meantime, the intraparticle diffusion model and Elovich model were also used to study the adsorption dynamics. The Langmuir isotherm model could be used to describe the adsorption process and the thermodynamic parameters Gibbs free energy ( $\Delta G^\circ$ ), standard enthalpy change ( $\Delta H^\circ$ ), and standard entropy change ( $\Delta S^\circ$ ) for the process were calculated. Furthermore, the Ti/CTS could be regenerated through desorption of the uranium and could be reused for adsorption.

*Keywords:* Adsorption; Uranyl ions removal; Aquatic medium; Ammonium fluotitanate; Chitosan

### 1. Introduction

With the rapid development of the world economy, the shortage of energy received more and more attention [1,2]. The nuclear energy, as a nonfossil fuels, is the only new energy sources which can cosmically substitute fossil fuels [3]. Uranium resources are the core of the development of nuclear energy [4]. The production of the uranium mining is also on the increase year by year. However, it generated huge amounts of radioactive wastewater with U(VI) [5]. Once the radioactive wastewater is released to the environment, the surface water and groundwater will be contaminated [6]. U(VI) in the surface water and groundwater, even at low concentrations, can be accumulated in organisms. Because

of the high chemical toxicity and radioactivity, it can cause severely irreversible skin, lung, bladder, and kidney damage, eventually leading to cancer when human ingested it [7–9]. Therefore, radioactive wastewater must be treated before being discharged. To reduce the environmental pollution, the efficient removal of uranium from aqueous solutions has received great attentions. At present, several techniques, such as chemical precipitation, solvent extraction, micellar ultra-filtration, organic and inorganic ion exchange, flotation, and adsorption have been developed [10]. Among them, adsorption is considered as a high-efficiency approach owing to its low-cost, high efficiency, and ease of operation [11]. Today, the adsorptions of metal ions such as U(VI) [12], Hg(II) [13,14], Th(IV) [12], and Cr(VI) [15] have increasingly become a research hotspot, at the same time, the uptake of the drugs [16] and the dyes such as methylene blue [17], methyl orange, Congo red [18], and Coomassie brilliant blue [19] is also the focus of research in this direction. The study of adsorbent

\* Corresponding author.

materials is very important for the governance of the future environment [20,21]. Recently, a variety of adsorbents have been developed including magnetic materials, fiber, metal-organic frameworks, and biopolymer polymers materials [22]. Among them, the biopolymer materials have received particular attention, especially chitosan [23]. The chitosan is the deacetylated product of chitin (a linear polymer of *N*-acetyl-d-glucosamine). It has a large number of functional groups such as amino and hydroxyl groups [24]. Due to the special structure, chitosan is unique among biopolymer with its high affinity for heavy metal ions through different mechanisms, including ion-exchange, chelation, and electrostatic attraction [25–28]. There is an abundance of citations in literatures describing the performance of chitosan as an adsorbent for pollutants from wastewater which included metals [29–33], dyes [34], phenols, fluoride, and phthalates. However, adsorbents based on chitosan and its derivatives have weak mechanical properties, the poor porosity, and chemical resistances, which may restrict its applications [35–38]. For these reasons, many researches have been drawn to improve the properties of the chitosan-based adsorbents [39,40]. This was mainly done to improve kinetics and fixation capacities of the polymer either by chemical or physical modifications [41]. To develop and modify for adsorption, for example, titanium [42], iron [43], aluminum [44], magnesium [45], and other metallic compounds are incorporated into chitosan.

In view of the above, to develop a low-cost and efficient novel composite adsorbent with high adsorption capacity for uranyl, our laboratory chose chitosan for the study. It is cross-linked by the glutaraldehyde to improve the chemical stability and  $(\text{NH}_4)_2\text{TiF}_6$  is doped to increase the nitrogen content and improve the adsorption capacity. By the one-pot method, the cross-linking chitosan submicron particles modified by ammonium fluotitanate (Ti/CTS) were synthesized.

The new adsorbent Ti/CTS was characterized by Fourier transform infrared spectroscopy, scanning electron microscope (SEM), Brunauer–Emmett–Teller (BET), and X-ray diffraction (XRD) techniques.

## 2. Experimental section

Caution! Although all of the uranyl compounds used in these studies contained depleted uranium salts, standard precautions were performed for handling radioactive materials, and all studies were conducted in a laboratory dedicated to studies on actinide elements.

### 2.1. Reagents

Analytical grade chemicals were used without further purification in this study. Chitosan and  $(\text{NH}_4)_2\text{TiF}_6$  (98%) was purchased from Aladdin Chemical Reagent Co., Ltd., P.R. China. Glutaric dialdehyde (50%) was obtained from Tianjin Damao Chemical Reagent Co., Ltd., P.R. China. Acetic acid (99.5%) was purchased from Tianjin FuYuHuaGong Chemical Reagent Co., Ltd., P.R. China. The stock solutions of uranium(VI) was prepared by dissolving uranyl (VI) nitrate ( $\text{UO}_2(\text{NO}_3)_2 \cdot 6\text{H}_2\text{O}$ ) (99.9%, which was obtained from Hu Bei JuShengWei Chemical Reagent Co, Ltd, P.R. China) in double distilled water at the desired initial concentration.

### 2.2. Preparation of Ti/CTS

Ti/CTS was prepared by the one-pot method with chitosan,  $(\text{NH}_4)_2\text{TiF}_6$ , and glutaric dialdehyde as main materials in an isothermal water bath at 40°C as shown in Fig. 1. Chitosan (1 g) was dissolved in 2% acetic acid solution (100 mL) with stirring until completely dissolved.

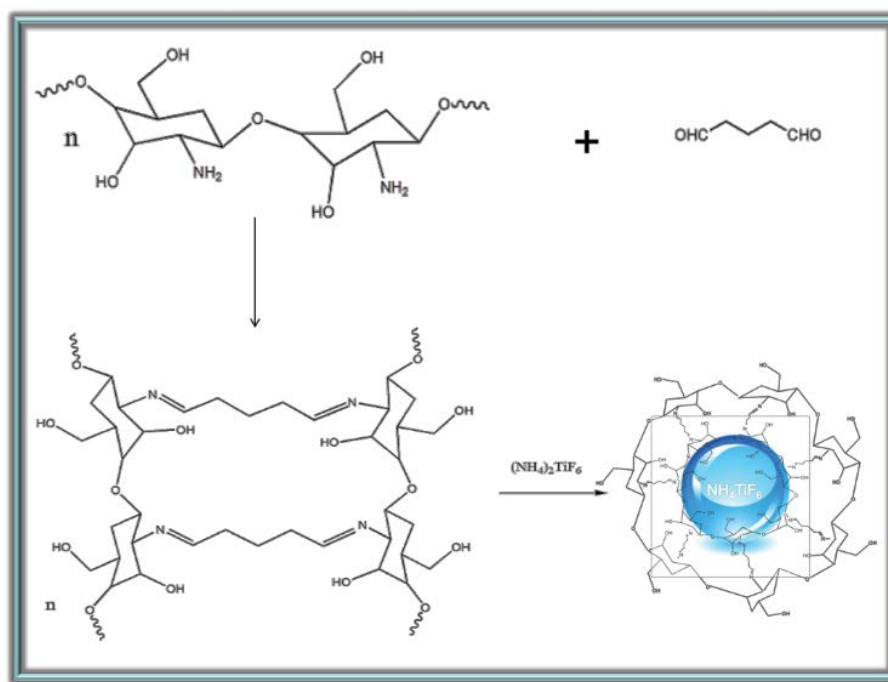


Fig. 1. The schematic illustration of the synthesis route to Ti/CTS.

Glutaraldehyde in ethanol as cross-linking reagent with the ratio of 1/10 (w/w of cross-linker to chitosan) was added dropwise into the chitosan solution to form a gel solution. Then the solution of ammonium fluotitanate (0.5–2 g in 20 mL water) was added slowly. The mixed solution was placed in an isothermal water bath at 40°C for 4 h. The pH was adjusted to 10 with 0.5 M NaOH. Then the production was separated by filter, fully washed with water and EtOH several times and dried at 80°C.

### 2.3. Physical measurements

X-ray powder diffraction patterns were obtained on a Bruker Advance-D8 equipped with Cu-K $\alpha$  radiation, in the range  $5^\circ < 2\theta < 55^\circ$ , with a step size of  $0.02^\circ$  ( $2\theta$ ) and a count time of 2 s per step. All IR measurements were obtained using a Bruker AXS TENSOR-27 FT-IR spectrometer with pressed KBr pellets in the range of  $400\text{--}4,000\text{ cm}^{-1}$  at room temperature. UV-vis absorption spectra were recorded with UV-1000 spectrometer (200–800 nm, in the form of liquid sample). The size and morphology of the material was investigated using scanning electron microscope and X-ray analyzer (SEM, KYKY-1000B). The specific surface area and the pore size were measured with the BET method using a Quantachrome Nova 3000 (Quantachrome Instruments, USA) multipoint gas adsorption analyzer at the liquid nitrogen temperature.

### 2.4. Removal of uranium ion

Batch experiments were performed to investigate the adsorption behavior of Ti/CTS toward  $\text{UO}_2^{2+}$  (VI). The  $\text{UO}_2^{2+}$  was analyzed by arsenazo III using a UV-vis spectrophotometer at 652 nm. 0.1 g of the adsorbent was equilibrated with 10 mL of  $\text{UO}_2^{2+}$  in the concentration range of  $0.05\text{--}0.55\text{ mg mL}^{-1}$ . The pH of solution was adjusted by 0.5 M  $\text{HNO}_3$  and 0.5 M NaOH. The adsorption capacity  $Q_e$  ( $\text{mg g}^{-1}$ ) was calculated according to Eq. (1) as follows:

$$Q_e = \frac{C_0 - C_e}{m} \times V \quad (1)$$

where  $Q_e$  is the adsorption capacity of adsorbent,  $C_0$  ( $\text{mg L}^{-1}$ ) and  $C_e$  ( $\text{mg L}^{-1}$ ) are initial concentration and equilibrium concentration, respectively.  $V$  (L) is the volume of the solution and  $m$  is the weight of Ti/CTS.

## 3. Results and discussion

### 3.1. Composition characterization of the Ti/CTS material

XRD was an effective method to provide the information about the physical and chemical form of the submicron ammonium fluotitanate embedded in chitosan matrix. The structure of chitosan molecules in nature contained plenty of hydroxyl and amino groups which may form strong intermolecular and intramolecular hydrogen bonds. As a result, chitosan molecules can form crystalline regions easily and exhibit the distinct crystalline peaks in the XRD patterns. While, after the chitosan was cross-linked by glutaraldehyde, it could destroy hydrogen bond between chitosan molecules and restrict the activity of the polymers. Therefore

the crystallization ability of the polymers was reduced and resulted in the weakness of the characteristic peaks of cross-linking chitosan as shown in Fig. 2 [25,46,47]. Several diffraction peaks cannot be detected from XRD pattern of cross-linking chitosan (crossed by glutaraldehyde) except two broad peaks at  $15^\circ$  and  $29^\circ$ , indicating that cross-linking chitosan was amorphous. The comparison of XRD pattern of Ti/CTS is illustrated in Fig. 2(b). There were two broad peaks, which were similar to the cross-linking chitosan. In addition, the characteristic sharp peaks at (100), (001), (101), (110), (200), (111), (002), (201), (102), (210), and (112) were also observed, which was in good agreement with the XRD spectrum of  $(\text{NH}_4)_2\text{TiF}_6$ . These characteristics corresponded to the existence of  $(\text{NH}_4)_2\text{TiF}_6$  in the structure which confirmed that there is the ammonium fluotitanate phase in the Ti/CTS structure.

To further investigate the structure of Ti/CTS, infrared spectroscopy was used for characterizing the functional groups on the sorbent at the different steps of the synthetic procedure (Fig. 3). From the cross-linked chitosan (Fig. 3(b)), it was found that the broad absorption bands centered in region of  $3,445\text{ cm}^{-1}$  were referred to the O–H and N–H stretching vibrations. The band of  $\nu_{\text{C-H}}$  was varied at approximately  $2,198\text{ cm}^{-1}$ . Features of the vibration modes of  $\text{C=N}$  were obtained at  $1,642$  and  $1,603\text{ cm}^{-1}$ , as expected. The narrow absorption band at  $1,427\text{ cm}^{-1}$  belonged to the band vibration of the N–H. Feature of the  $\nu_{\text{C-H}}$  vibration modes of  $\text{CH}_2$  in  $\text{CH}_2\text{OH}$  was obtained at  $1,379\text{ cm}^{-1}$ . The narrow absorption bands at  $1,320$  and  $1,155\text{ cm}^{-1}$  belonged to the stretching vibration of the C–N. The bands at  $1,076$  and  $901\text{ cm}^{-1}$  were attributed to the characteristic stretching vibrations of the C–O which may be overlapped partially by the asymmetric stretching vibrations of the C–N [48]. The IR was also tested for Ti/CTS, as shown in Fig. 3(c). Comparing the cross-linked chitosan, it was found the similar spectra characteristic of cross-linked chitosan with subtle, yet significant, differences. Slight blue shift of the absorbing peaks and change of the intensity were observed. The changing band in the higher wavenumber at  $3,427\text{ cm}^{-1}$  was blue shift to the cross-linked

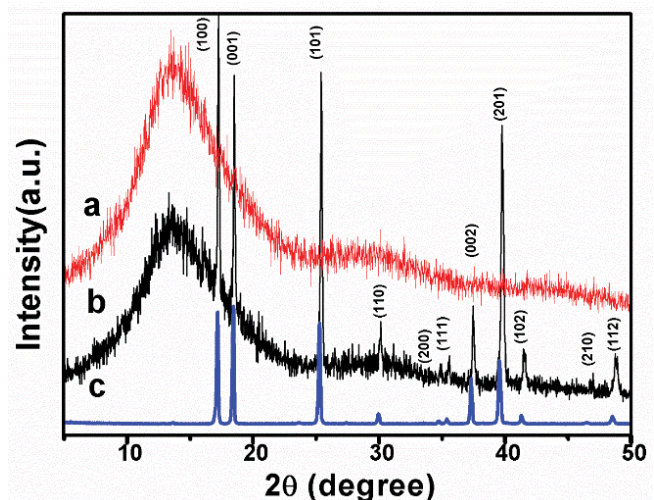


Fig. 2. The XRD spectrum of (a) cross-linking chitosan, (b) Ti/CTS, and (c)  $(\text{NH}_4)_2\text{TiF}_6$ .

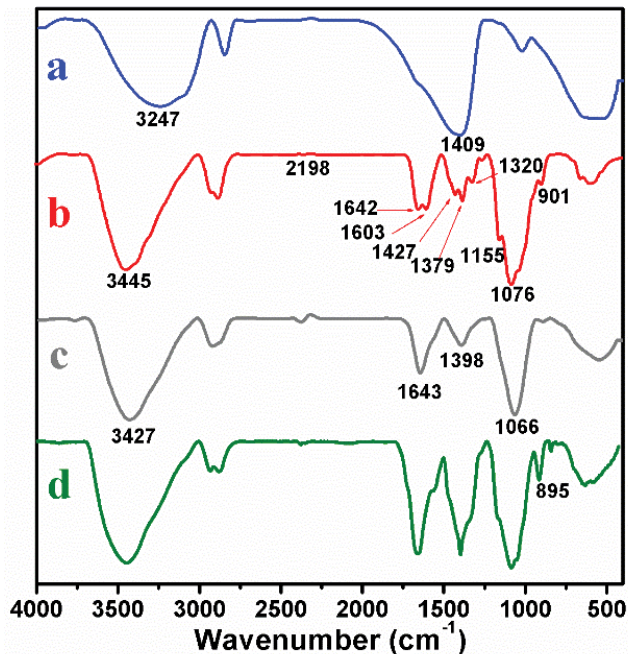


Fig. 3. The IR spectrum of (a)  $(\text{NH}_4)_2\text{TiF}_6$ , (b) cross-linking chitosan, (c) Ti/CTS, and (d) Ti/CTS after  $\text{UO}_2^{2+}$  adsorbed.

chitosan about  $27\text{ cm}^{-1}$ . It could be due to the increased amide from  $(\text{NH}_4)_2\text{TiF}_6$ , which also increased hydrogen bonding as has been shown before. Within the lower wavenumber range of  $500\text{--}1,800\text{ cm}^{-1}$ , the most significant changes were from the decrease and sharpening of the peaks at  $1,643$  and  $1,398\text{ cm}^{-1}$ , as well as disappearing of the shoulder peaks at  $1,066\text{ cm}^{-1}$ . The disappearing of the split and the blue shift were both the proof of the change in the material structure which may be because of the existence of  $(\text{NH}_4)_2\text{TiF}_6$  on the chitosan. The IR of Ti/CTS after  $\text{UO}_2^{2+}$  adsorbed is shown in Fig. 3(d), the

peak of  $895\text{ cm}^{-1}$  was significantly enhanced, which proves that there is the uranyl ion in the structure.

The scan electron micrographs of the composite material Ti/CTS (with the mass ratio of chitosan/ $(\text{NH}_4)_2\text{TiF}_6$ : 4:1 (a), 2:1 (b), 4:3 (c), and 1:1 (d)), cross-linked chitosan (e), the magnification of (c) with the magnifying power of 220k (f), and Ti/CTS after uranyl adsorption (g) are shown in Fig. 4. The cross-linked chitosan was the porous solids and exhibited a regular and smoother surface. The scale of the obtained layer was  $10\text{ }\mu\text{m}$  thick with large specific surface area and high porosity. When the  $(\text{NH}_4)_2\text{TiF}_6$  was doped in the cross-linked chitosan, it was shown that the ball-like structure was formed in the surface layer. It may be because the  $(\text{NH}_4)_2\text{TiF}_6$  can organize to form spherical globules with around  $200\text{ nm}$  outer diameter as shown in Fig. 4(f). As the increase of mass ratio, the  $(\text{NH}_4)_2\text{TiF}_6$  submicron particle was increased. When the ratio was 4:3, surfaces of the chitosan were almost coated with the  $(\text{NH}_4)_2\text{TiF}_6$  submicron particle. When the ratio was 1:1, the  $(\text{NH}_4)_2\text{TiF}_6$  submicron particle was completely casted with the  $(\text{NH}_4)_2\text{TiF}_6$  submicron particle. The structure of Ti/CTS after uranyl adsorption had almost same structure, which indicated that Ti/CTS can still maintain its surface structure after adsorption for 5 h. Further, elemental maps of C, O, N, and U and their collective map are given as Fig. 4(h). This was in good agreement with the proposed structure of Ti/CTS and further indicated that the  $(\text{NH}_4)_2\text{TiF}_6$  was successfully mixed in the Ti/CTS. The U energy spectra map was correlated with those of O and N energy spectra maps, which implied the tentative affinity of uranyl ions with the adsorbent.

To further study the structure of the Ti/CTS, the pore structure and surface area had been analyzed by nitrogen adsorption methods. A typical IV  $\text{N}_2$  adsorption/desorption isotherm can be seen in Fig. S1(a). The inflection point was found at a relative pressure  $P/P_0$  ranging from 0 to 0.1, which can reveal the existence of micropores. A distinct hysteresis loop, observed in the range from 0.1 to  $1(P/P_0)$ , was classified

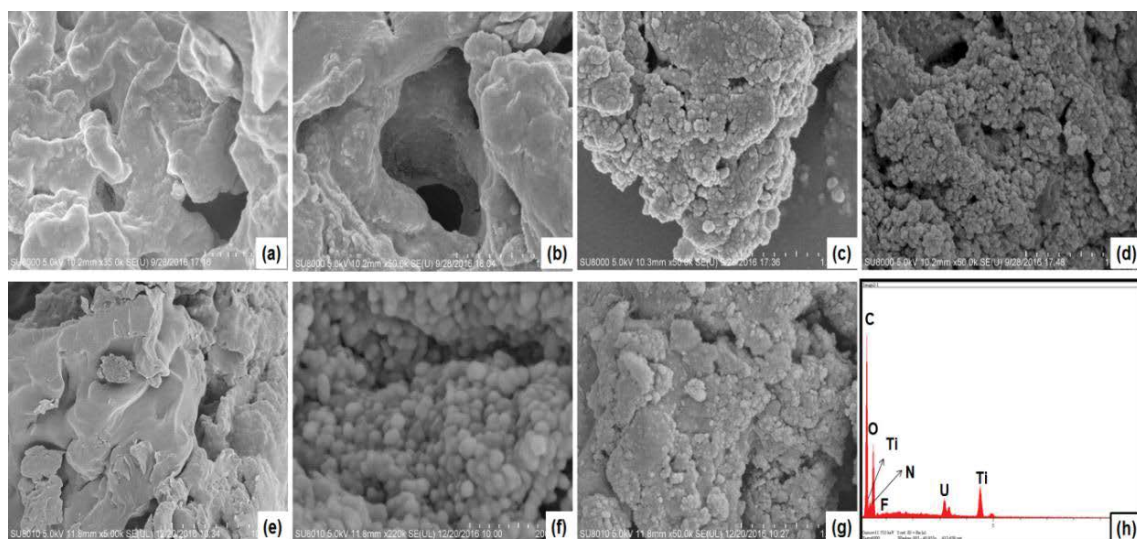


Fig. 4. The SEM of the composite material Ti/CTS (with the mass ratio of chitosan/ $(\text{NH}_4)_2\text{TiF}_6$ : 4:1 (a), 2:1 (b), 4:3 (c), 1:1 (d)), cross-linked chitosan (e), the magnification of (c) with the magnifying power of 220k (f), elemental mapping of uranyl ion adsorbed on Ti/CTS (g), and EDAX spectrum of uranyl ions adsorbed Ti/CTS (h).

as type H1. It may represent that there were particle homogeneously dispersed in the Ti/CTS, which was in good consistent with the observed in SEM. The surface area and pore volume of Ti/CTS were  $98.841 \text{ m}^2 \text{ g}^{-1}$  and  $0.1527 \text{ cm}^3 \text{ g}^{-1}$ , respectively. The pore size distribution curve is with an average pore size of  $1.9319 \text{ nm}$  (Fig. S1(b)). This shows that Ti/CTS is a porous solid material [49–51].

### 3.2. Study on the Ti/CTS material for uranium adsorption behavior

#### 3.2.1. Effect of mass ratio of Ti/CTS on $\text{UO}_2^{2+}$ adsorption

In order to enhance the adsorption capacity of the Ti/CTS, a series of experiments about equilibrium adsorption property of Ti/CTS with different mass ratio were carried out. The results of the experiment can be seen from Fig. 5. The experiment conditions were:  $20 \text{ mL}$  solution,  $0.5 \text{ mg mL}^{-1}$  U (VI),  $5 \text{ h}$  stirring time, and  $25^\circ\text{C}$ . After tests, Ti/CTS with different synthesis mass ratio (1:4, 2:4, 3:4, and 4:4) possessed different adsorption properties. The equilibrium adsorption ability was better when the mass ratio of  $(\text{NH}_4)_2\text{TiF}_6/\text{chitosan}$  was 3:4. It might be due to amounts of the doped  $(\text{NH}_4)_2\text{TiF}_6$  could promote the ability of adsorbent. After nimiety  $(\text{NH}_4)_2\text{TiF}_6$  was doped in the Ti/CTS, the surface of the chitosan was covered, which may hinder the effect between hydroxyl and metal ions and cause decreased the adsorption ability. This was consistent with the observation from SEM. In the following test, based on the earlier result, we thought the optimum condition to synthesize Ti/CTS was 3:4.

#### 3.2.2. Effect of pH on $\text{UO}_2^{2+}$ adsorption

The pH value of the aqueous solution, as one of the most important parameters, can influence the chemical properties of uranium(VI) and the adsorbents, which played an important role in the whole sorption process and particularly on sorption capacity. On the one hand,  $\text{UO}_2^{2+}$  cation was unstable enough under strong acid and strong base, which tended to hydrolyze and polymerize, forming a number of polynuclear uranyl species, and even generated hydroxide precipitation [4], as Fig. 6 illustrates. On the other hand, it

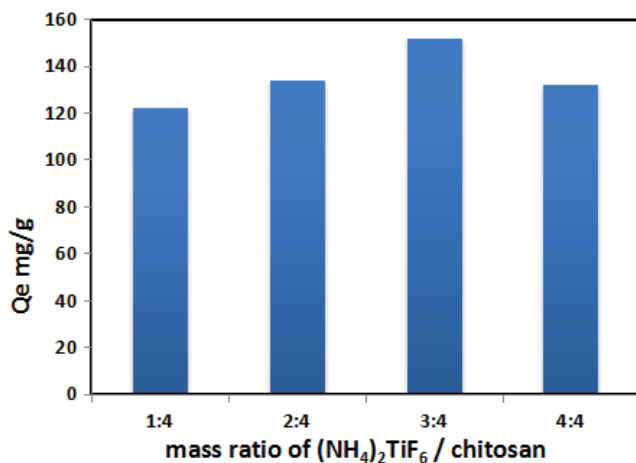


Fig. 5. Effect of mass ratio on adsorption ability of Ti/CTS.

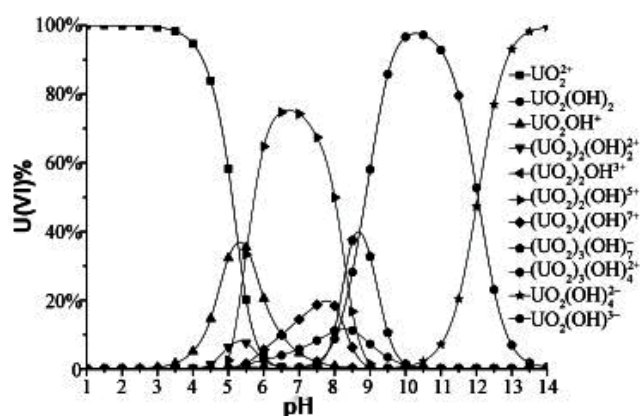


Fig. 6. U(VI) various species distribution as a function of pH at  $25^\circ\text{C}$ .

may influence the surface charge and the dissociation of functional groups which presented at the surface of the sorbent such as hydroxyl and amino groups [9]. The adsorbents of uranium(VI) on Ti/CTS was investigated using  $0.05 \text{ g}$  adsorbent and  $20 \text{ mL}$   $\text{UO}_2^{2+}$ (VI) ( $0.05 \text{ mg L}^{-1}$ ) over a range of pH values from 2 to 10. The pH of the solution was adjusted to the required value by the solution of  $\text{HNO}_3$  and  $\text{NaOH}$ . The results are shown in Fig. 7. The equilibrium adsorption property of uranyl in each pH value indicated the strong impact of pH on adsorption capacity. The equilibrium adsorption ability increased with increasing pH, to a maximum value of pH 7.0, where  $Q_e$  was  $208.25 \text{ mg mL}^{-1}$  and most of the uranyl ions was extracted from solution. Then a slight decline tendency in removal efficiency was observed at pH 8–9. After that, the declined trend is more rapid at pH 10. When the solution was strongly acid, the relative low sorption capacity of Ti/CTS may be due to surface protonation reaction. It was generally accepted that more protons would be available to be protonated and to form  $\text{H}_3\text{O}^+$  groups, which competed with  $\text{UO}_2^{2+}$  for adsorption sites and then reducing the number of binding sites for the adsorption of  $\text{UO}_2^{2+}$  were reduced. With the increasing of the concentration of hydroxyl, uranyl ion formed stable complexes with hydroxyl such as  $\text{UO}_2(\text{CO}_3)_3(\text{OH})_3^-$  and  $\text{UO}_4(\text{OH})_7^-$ . These ions

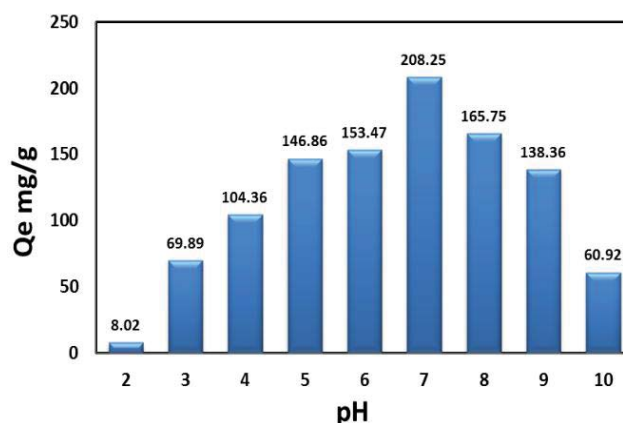


Fig. 7. Effect of initial pH on adsorption ability of Ti/CTS.

can form more stable hydrogen bond with amino, hydroxyl, fluotitanic acid anion and other functional group at the surface of Ti/CTS which was helpful for the absorption. At higher pH, the uranium was direct precipitation from the uranium solution.  $\text{NH}_4^+$  left the surface of the Ti/CTS and progressively deprotonated.  $\text{UO}_2(\text{OH})_2$ , as a stable precipitation product, can also form. Both of them caused decrease of the interaction between Ti/CTS and  $\text{UO}_2^{2+}$ , and then led to the decrease in removal efficiency. Therefore, according to analysis result above, pH 6.0 was selected for the further experiments.

### 3.2.3. Effect of the amount of the sorbent on Ti/CTS for $\text{UO}_2^{2+}$ adsorption

The effect of the dosage of Ti/CTS on the uranium removal is shown in Fig. 8. The removal efficiency clearly increases when the amount of the Ti/CTS was increased from 0.01 to 0.025 g. That may be because the more dosage of sorption was in the solution, the more active sites can attract the uranium. The amounts of uranium removal approached equilibrium (99%) when 0.025g Ti/CTS was used. The overdose Ti/CTS cannot obviously increase the amounts of uranium removal. In considering the removal efficiency, the dosage of 0.025 g was considered as an optimum dose and is used for further study.

### 3.2.4. Effect of contact time and adsorption dynamics for $\text{UO}_2^{2+}$ adsorption

Fig. 9 shows the relationship between the adsorption capacity and the contact time. The adsorption time was examined from 15 to 500 min at 25°C. There were two stages in adsorption process: an initial rapid stage and a slower approach to equilibrium phase stage. At the first stage, it was clear that the adsorption capacity increased with the contact time. The rate of adsorption was increasing rapidly which can be interpreted to the instantaneous adsorption stage or external surface adsorption process. The second stage was also known as the gradual adsorption process, the adsorption rate was slower. With the decrease of active sites, the rate of adsorption gradually reduced where intraparticle diffusion

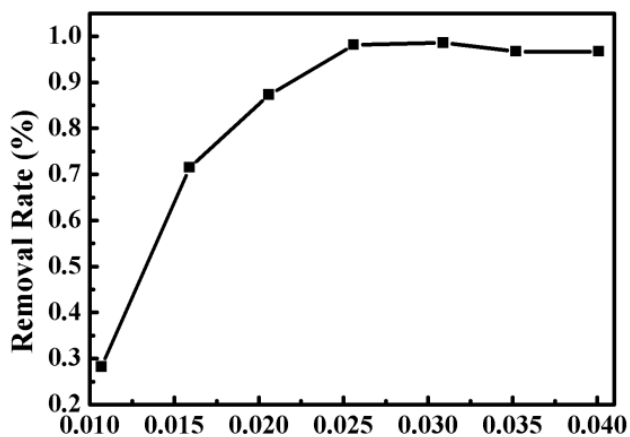


Fig. 8. Effect of amount of sorbent on adsorption of uranium by Ti/CTS.

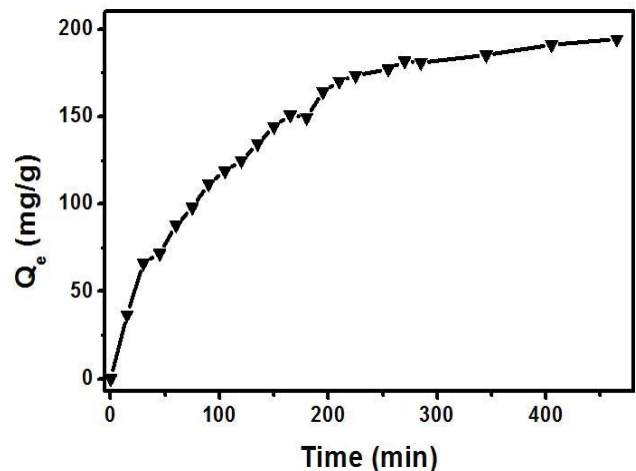


Fig. 9. Effect of contact time on uranium(VI) adsorption.

controlled the adsorption rate. Then the adsorption reached equilibrium. Finally, it was found that the change of adsorption capacities for uranium did not show notable effects, which proved adsorption to uranium reached equilibrium after 300 min. It can be seen that the 300 min was enough to reach sorption equilibration. So the follow-up experiments were carried out for 300 min.

It was generally accepted that most adsorption reactions took place through multistep mechanism comprising (1) external film diffusion, (2) intraparticle diffusion, and (3) interaction between adsorbate and active site [52]. To investigate the kinetic mechanism of the adsorption process, the adsorption data was analyzed using the pseudo-first-order kinetic, pseudo-second-order models, intraparticle diffusion models, and the Elovich model. The pseudo-first-order kinetic (Eq. (2)), also called Lagergren model, was given as follows:

$$\log(Q_e - Q_t) = \log Q_e - \frac{k_1 t}{2.303} \quad (2)$$

where  $Q_e$  and  $Q_t$  ( $\text{mg g}^{-1}$ ) are the adsorption capacity at equilibrium and at time, and  $k_1$  is the rate for the pseudo-first-order kinetic.

The pseudo-second-order models can be shown as follows:

$$\frac{t}{Q_t} = \frac{1}{Q_e^2 k_2} + \frac{t}{Q_e} \quad (3)$$

where  $Q_e$  and  $Q_t$  ( $\text{mg g}^{-1}$ ) are the same as the pseudo-first-order kinetic, and the  $k_2$  is the rate for the pseudo-second-order kinetic. To calculate the initial adsorption rate  $h$ , Eq. (4) can be used with  $k_2$  and  $Q_e$  as follows:

$$h = k_2 Q_e^2 \quad (4)$$

The intraparticle diffusion model was expressed as follows:

$$Q_t = k_p t^{1/2} + C \quad (5)$$

where  $k_p$  is the intraparticle diffusion rate ( $\text{mg g}^{-1} \text{min}^{-0.5}$ ) and  $C$  is a constant related to the boundary layer thickness which is the intercept for the linear “ $t^{1/2}$  versus  $Q_t$ ” of the adsorption.

The Elovich model can be obtained by Eq. (6) as follows:

$$Q_t = \alpha \ln(\alpha\beta) + \alpha \ln t \quad (6)$$

where  $\alpha$  in this model is the initial adsorption rate ( $\text{mmol g}^{-1} \text{min}^{-1}$ ).  $\beta$  is related to the extent of surface coverage. The data of adsorption were fitted by four kinetic models and shown in Fig. S2(a)–(d). The parameters for each model were calculated and listed in Table 1.

The values of  $Q_c$  and  $k_1$  for pseudo-first-order model were calculated from the intercepts and slopes of the “ $\log(Q_c - Q_t)$  versus  $t$ ” plot. The low-related coefficient  $R^2$  (0.9800) and the large difference between the calculated values of adsorption capacity and the experimental values indicated that the sorption mechanism of uranium(VI) on Ti/CTS did not base on a pseudo-first-order kinetic model and hence the adsorption was not diffusion controlled. While when the pseudo-second-order model was employed, the linear fit of the plot of  $t/Q_t$  versus  $t$  revealed high correlation coefficient ( $R^2 = 0.9933$ ). The  $k_2$  value, determined from the intercept of the plot, was  $1.776 \times 10^{-5}$ . Furthermore the experimental data were more closely agreed with the calculating equilibrium adsorption capacity values for the pseudo-second-order model than the one for pseudo-first-order model. The parameter of the initial adsorption rate  $h$  calculated from the  $k_2$  and  $Q_c$  was  $1.007 \text{ g mg}^{-1} \text{min}^{-1}$ . Thus, it could be concluded that the sorption of U(VI) with Ti/CTS followed the pseudo-second-order kinetics, which was based on the assumption that the rate-limiting step may be chemical sorption. It was

reasonable to inference that there were the covalent forces through sharing or exchange of electrons between sorbent and uranium. It can influence adsorption rate and the chemical affinity of uranyl ions. And the adsorption group was the rate limiting step for the sorption of U(IV) onto Ti/CTS. It was also noted that the small values of  $k^2$  was the proof that the rate of uranyl uptake decreased with time. As we all known, the solid absorption was affected by film diffusion or intraparticle diffusion [52]. From the two kinetic models, the adsorption of uranyl ions on Ti/CTS may be not due to diffusion. For further understanding the adsorption mechanism of Ti/CTS, the adsorption data were studied in view of intraparticle diffusion model (Fig. S2(c)). The plot of  $Q_t$  against  $t^{0.5}$  revealed two linear characteristics and both were high coincidence with the model, in which the correlation coefficient values ( $R^2$ ) were 0.9959 and 0.9920, respectively. The parameter  $C$  was a constant related to the boundary layer thickness. If the intercept  $C$  was zero so that the plot passed through the origin, the intraparticle diffusion was the sole rate-determining step. Since the region of the plot did not pass through the origin, it may be concluded that the adsorption of uranyl ions on Ti/CTS was complex. Not only surface adsorption contributed to the rate-determining step [9], but also the intraparticle. This is consistent with the observation from the pseudo-second-order model. The two parts of the line in Fig. S2(c) indicated that multiple steps influenced the mass transfer process. From the beginning to 225 min as the first step, with the small value of  $C$ , the diffusion occurred from bulk phase into pores with the adsorption at the exterior surface of adsorbent. The rate of the adsorption was fast and the initial straight line corresponded to the instantaneous adsorption due to film diffusion. Then at the equilibrium step, the rate of the adsorption decreased obviously and the adsorption of uranyl ions was not based on diffusion mechanism. It may attribute to the interaction between the adsorbate and the active site. To attest it, the Elovich model which can announce the irregularities of the data that other kinetic equations ignore was used as shown in Fig. S2(d). It is commonly used to describe the sorption behavior with a rapid equilibrium rate in early period, and then the rate slowed down at later periods of the sorption.  $\alpha$  and  $\beta$  represented the rate of sorption and surface coverage was calculated for 51.74 and  $2.062 \times 10^{-3}$ , respectively. The data can fit the model well with the correlation coefficient value ( $R^2$ ) 0.9751. From the four kinetic models, the process of ion adsorption in the whole reaction was controlled by liquid film diffusion and intraparticle diffusion. And because of the loose hollow internal structure of the Ti/CTS,  $\text{UO}_2^{2+}$  can diffuse easily to the inner surface, which also indicated the intraparticle diffusion is not a rate-limiting step. Furthermore, Ti/CTS using chitosan as substrate, had a large number of amine and hydroxyl groups that are responsible for  $\text{UO}_2^{2+}$  binding via chelation mechanisms.

### 3.3. Sorption isotherms and adsorption thermodynamics

It was well established that the amount of adsorption was a function of concentration when the temperature was constant in the solid–liquid adsorption system, which is also called the adsorption isotherms. The adsorption isotherms can be expressed by the linear in which  $Q_c$  was the vertical axis and

Table 1  
Kinetic parameters for  $\text{UO}_2^{2+}$  adsorption onto Ti/CTS

	Parameters
Pseudo-first order	
$Q_{\text{cal}}$ ( $\text{mol kg}^{-1}$ )	170.0
$k_1$ ( $\text{min}^{-1}$ )	$6.909 \times 10^2$
$R^2$	0.9800
Pseudo-second order	
$Q_{\text{cal}}$ ( $\text{mol kg}^{-1}$ )	238.1
$k_2$ ( $\text{g mg}^{-1} \text{min}^{-1}$ )	$1.776 \times 10^{-5}$
$R^2$	0.9933
Intraparticle diffusion	
$K_{1p}$ ( $\text{mg g}^{-1} \text{min}^{-0.5}$ )	12.20
$C_1$	-6.793
$R^2$	0.9959
$K_{2p}$ ( $\text{mg g}^{-1} \text{min}^{-0.5}$ )	3.186
$C_2$	126.3
$R^2$	0.9920
Elovich model	
$\alpha$	51.74
$\beta$	$2.062 \times 10^{-3}$
$R^2$	0.9751

$C_e$  was the horizontal axis. Through the shape of the sorption isotherms, the surface structure of the porous solid, the pore structure as well as the interaction between the adsorbent and the adsorbate can be compendious and clearly reflected. The adsorption of uranyl ions on Ti/CTS was in terms of Freundlich and Langmuir adsorption isotherms at temperatures of 298, 308, and 318 K shown in Fig. S3. The adsorption of uranium on Ti/CTS increased when temperature was increased to demonstrate that uranium removal by adsorption favored a high temperature. Adsorption equilibrium data have been subjected by using Langmuir and Freundlich isotherms at various temperatures. The Freundlich isotherm was appropriate for the monomolecular layer at the heterogenous surface and the linear form of it is represented in Eq. (7) as follows:

$$\log Q_e = \log K_f + \frac{1}{n} \log C_e \quad (7)$$

where  $K_f$  is the Freundlich isotherm constant, and  $1/n$  is related to the heterogeneity parameter of the sorbent and indicated strength of adsorption in the adsorption process [53]. The linear fit of the plot of  $\log(Q_e)$  versus  $\log(C_e)$  was poorly correlated ( $R^2$  between 0.9415 and 0.9710), as shown in Table 2. It can be inferred that the adsorption of uranyl ions on Ti/CTS was not based on Freundlich isotherm model. The data  $1/n$  and  $K_f$  can be calculated as shown in Table 2. The values of  $1/n$  were all ranged between 0 and 1 indicating the strong interaction of U(VI) ions with the adsorbent. Then the adsorption data obtained were fitted to Langmuir isotherm model which had formed as shown in Eq. (8) as follows:

$$\frac{C_e}{Q_e} = \frac{1}{K_L Q_{\max}} + \frac{C_e}{Q_{\max}} \quad (8)$$

The  $K_L$  is a constant related to the adsorption energy ( $L \text{ mg}^{-1}$ ). The values of maximum adsorption capacity ( $Q_{\max}$ ) and Langmuir constant ( $K_L$ ) were evaluated from the intercept and slope of the Langmuir plots. It was observed that Langmuir isotherm model yielded better fit to the experimental data and had higher correlation coefficients compared with those for Freundlich. With the  $K_L$ , another parameter  $R_L$  which indicated the type of isotherm to be favorable was defined in Eq. (9) as follows:

$$R_L = \frac{1}{1 + (1 + K_L C_0)} \quad (9)$$

where  $C_0$  is the initial metal concentration. For an initial concentration of  $0.5 \text{ mg mL}^{-1}$ , the  $R_L$  was found. As shown in Table 2, the value of  $R_L$  was between 0 and 1 indicated the adsorption was favorable. Notably, the adsorption of uranium(VI) increased with the increasing of temperature, which indicated the endothermic nature of the process. To evaluate it, the thermodynamic parameters were calculated using Eq. (10) as follows:

$$\ln K = \frac{\Delta S^\circ}{R} - \frac{\Delta H^\circ}{RT} \quad (10)$$

where  $R$  is the gas constant ( $8.314 \text{ J mol}^{-1} \text{ K}^{-1}$ ) and  $T$  is the absolute temperature (K),  $\Delta S$  is standard entropy ( $\text{J mol}^{-1} \text{ K}^{-1}$ ),  $\Delta H^\circ$  is standard enthalpy ( $\text{kJ mol}^{-1}$ ). The values of  $\Delta H^\circ$  and

Table 2  
Isotherm constants for  $\text{UO}_2^{2+}$  adsorption onto Ti/CTS

Temperature (K)		298	308	318
Langmuir	$Q_e$	181.1	200.3	218.0
	$K_L$	12.27	13.71	18.39
	$R^2$	0.9950	0.9990	0.9916
	$R_L$	0.1402	0.1273	0.09809
Freundlich	$n$	0.2456	0.4324	0.2843
	$K_f$	2.147	2.650	2.607
	$R^2$	0.9415	0.9672	0.9710

$\Delta S^\circ$  were evaluated from the intercept and slope of the linear plot (Fig. S4). The standard free energy values ( $\Delta G^\circ$ ) were calculated by Eq. (11) as follows:

$$\Delta G^\circ = -RT \ln K_L \quad (11)$$

As data of  $\Delta S^\circ$ ,  $\Delta H^\circ$ , and  $\Delta G^\circ$  were listed in Table S1, the negative  $\Delta G^\circ$  can demonstrate the adsorption process was spontaneous [8].

#### 3.4. Sorption mechanism of $\text{UO}_2^{2+}$ on the material of Ti/CTS

To study what the role the existence of ammonium fluotitanate played in the sorption process, the adsorption capacity of cross-linked chitosan toward  $\text{UO}_2^{2+}$  was studied. The equilibrium adsorption capacity was  $98 \text{ mg g}^{-1}$  which was far below the equilibrium adsorption capacity of Ti/CTS. According to the analysis of the structure and the study of the adsorption kinetic as well as the thermodynamics, the adsorption mechanism of the Ti/CTS might be attributed to both ion exchange and electron donating acceptor coupling reactions at the surface sites. First, the  $-\text{OH}$ ,  $-\text{NH}_2$ , and other functional groups on the surface of the cross-linked chitosan in Ti/CTS can adsorb the  $\text{UO}_2^{2+}$  by surface complexation and cation exchange mechanisms, and the relative large surface area and pore diameter of the chitosan substrate can enhance the adsorption capacity. Second, the ammonium in the ammonium fluotitanate submicron particles can improve the amount of N-containing material. In the third part, the fluotitanate with the negative charge had strong electrostatic attraction toward the  $\text{UO}_2^{2+}$  group which was positively charged and fluorine ion in the structure enhances adsorption capacity by increasing the hydrogen bond force.

#### 3.5. Desorption studies of $\text{UO}_2^{2+}$ on the material of Ti/CTS

The reusability of Ti/CTS was tested with  $0.025 \text{ g Ti/CTS}$  which had been soaked in  $0.5 \text{ mg mL}^{-1} \text{ UO}_2^{2+}$  solution for 24 h. It is found that absorbed Ti/CTS material, which was eluted by  $0.5 \text{ M HNO}_3$  solution,  $0.5 \text{ M NaOH}$  and  $0.5 \text{ M EtOH}$  solution, successively, also has still some adsorption activity. And Ti/CTS material removal could still maintain more than 70% after repeated more than five times.

#### 3.6. Comparison of adsorption capacity for $\text{UO}_2^{2+}$ of Ti/CTS with reported adsorbents

The maximum sorption capacity of Ti/CTS and other adsorbents for  $\text{UO}_2^{2+}$  is compared in Table 3. (I), (II), (III), and

Table 3  
Comparison of adsorption capacity for  $\text{UO}_2^{2+}$  of Ti/CTS with reported adsorbents

Adsorbents	Metal ion or dye	Equilibration time (min)	Adsorption capacity ( $\text{mg g}^{-1}$ )/ uptake percentage	References
Magnetic chitosan (I)	U(VI)	40	42	[54]
Cross-linked chitosan with epichlorohydrin (II)	U(VI)	180	49.05	[55]
Ethylenediamine-modified magnetic chitosan (III)	U(VI)	30	82.83	[9]
Amine-functionalized magnetic-chitosan nano-based particles (IV)	U(VI)	40	177.93	[28]
Organic-inorganic hybrid thiostannate (V)	U(VI)	300	338.43	[56]
Multilayer titanate nanotubes (VI)	U(VI)	90	333	[57]
Cross-linking chitosan submicron particles modified by ammonium fluotitanate (VII)	U(VI)	300	195	This work

(IV) were slightly weaker than this work. (V) and (VI) had better adsorption capacity than this work. While, different functionalized modification adsorbents had different adsorption capacity. That may be because the adsorption capacity depends on the porosity, surface area, functional group in the structure, and the types of raw materials.

#### 4. Conclusion

Ammonium fluotitanate-functionalized cross-linking chitosan submicron-based particles (Ti/CTS) have been successfully synthesized and its application as an adsorbent for uranyl ions has been studied. The adsorption isotherm studies, kinetic studies, and thermodynamic studies indicated the mechanism was both the chemisorption and physisorption. The pseudo-second-order kinetic model was used to correlate the kinetic experimental data and the kinetic parameters were evaluated. The Langmuir and Freundlich models were applied to describe the adsorption isotherms. The values of  $\Delta H^\circ$ ,  $\Delta S^\circ$ , and  $\Delta G^\circ$  were calculated. The positive value of  $\Delta G^\circ$  indicated endothermic nature of adsorption. The adsorption behavior of Ti/CTS clearly indicated it was an effective and economic adsorbent for uranyl ions adsorption from aqueous solution with high adsorption capacity.

#### Acknowledgments

This work was supported by the grants of the National Natural Science Foundation of China (no. 21571091), Guangxi Key Laboratory of Information Materials, Guilin University of Electronic Technology, P.R. China (Project no. 151002-K), Commonwealth Research Foundation of Liaoning province in China (no. 20170055) for financial assistance.

#### References

- [1] J.S. Santos, L.S.G. Teixeira, W.N.L.D. Santos, V.A. Lemos, J.M. Godoy, S.L.C. Ferreira, Uranium determination using atomic spectrometric techniques: an overview, *Anal. Chim. Acta*, 674 (2010) 143–156.
- [2] X. Min, W. Yang, Y.F. Hui, C.Y. Gao, S. Dang, Z.M. Sun,  $\text{Fe}_3\text{O}_4@zif-8$ : a magnetic nanocomposite for highly efficient  $\text{UO}_2^{2+}$  adsorption and selective  $\text{UO}_2^{2+}/\text{Ln}^{3+}$  separation, *Chem. Commun.*, 53 (2017) 4199–4202.
- [3] W. Yang, T.G. Parker, Z.M. Sun, Structural chemistry of uranium phosphonates, *Coord. Chem. Rev.*, 303 (2015) 86–109.
- [4] A.R. Fox, S.C. Bart, K. Meyer, C.C. Cummins, Towards uranium catalysts, *Nature*, 455 (2008) 341–349.
- [5] Y. Lu, Uranium extraction: coordination chemistry in the ocean, *Nat. Chem.*, 6 (2014) 175–177.
- [6] M.B. Andersen, T. Elliott, H. Freymuth, K.W. Sims, Y. Niu, K.A. Kelley, The terrestrial uranium isotope cycle, *Nature*, 517 (2015) 356–359.
- [7] H. Yan, J. Bai, X. Chen, J. Wang, H. Zhang, Q. Liu, M. Zhang, L. Liu, High U(VI) adsorption capacity by mesoporous  $\text{Mg}(\text{OH})_2$  deriving from  $\text{MgO}$  hydrolysis, *RSC Adv.*, 3 (2013) 23278–23289.
- [8] C.R. Preetha, J.M. Gladis, T.P. Rao, G. Venkateswaran, Removal of toxic uranium from synthetic nuclear power reactor effluents using uranyl ion imprinted polymer particles, *Environ. Sci. Technol.*, 40 (2006) 3070–3074.
- [9] S. Xie, J. Yang, C. Chen, X. Zhang, Q. Wang, C. Zhang, Study on biosorption kinetics and thermodynamics of uranium by *Citrobacter freundii*, *J. Environ. Radioact.*, 99 (2008) 126–133.
- [10] Y. Liu, X. Cao, R. Hua, Y. Wang, Y. Liu, C. Pang, Y. Wang, Selective adsorption of uranyl ion on ion-imprinted chitosan/PVA cross-linked hydrogel, *Hydrometallurgy*, 104 (2010) 150–155.
- [11] S. Li, H. Bai, J. Wang, X. Jing, Q. Liu, M. Zhang, R. Chen, L. Liu, C. Jiao, In situ grown of nano-hydroxyapatite on magnetic CaAl-layered double hydroxides and its application in uranium removal, *Chem. Eng. J.*, 193–194 (2012) 372–380.
- [12] A.A. Alqadami, M. Naushad, Z.A. Allothman, A.A. Ghfar, Novel metal-organic framework (MOF) based composite material for the sequestration of U(VI) and Th(IV) metal ions from aqueous environment, *ACS Appl. Mater. Interfaces*, 9 (2017) 36026–36037.
- [13] M. Naushad, S. Vasudevan, G. Sharma, A. Kumar, Z.A. AlOthman, Adsorption kinetics, isotherms, and thermodynamic studies for  $\text{Hg}^{2+}$  adsorption from aqueous medium using alizarin red-S-loaded amberlite IRA-400 resin, *Desal. Wat. Treat.*, 57 (2016) 18551–18559.
- [14] M. Naushad, T. Ahamad, B.M. Al-Maswari, A.A. Alqadami, S.M. Alshehri, Nickel ferrite bearing nitrogen-doped mesoporous carbon as efficient adsorbent for the removal of highly toxic metal ion from aqueous medium, *Chem. Eng. J.*, 330 (2017) 1351–1360.
- [15] G. Sharma, M. Naushad, A.H. Al-Muhtaseb, A. Kumar, M.R. Khan, S. Kalia, Shweta, M. Bala, A. Sharma, Fabrication and characterization of chitosan-crosslinked-poly(alginate) nanohydrogel for adsorptive removal of Cr(VI) metal ion from aqueous medium, *Int. J. Biol. Macromol.*, 95 (2017) 484–493.
- [16] D. Pathania, D. Gupta, N.C. Kothiyal, G. Sharma, G.E. Eldesoky, M. Naushad, Preparation of a novel chitosan-g-poly(acrylamide)/Zn nanocomposite hydrogel and its applications for controlled drug delivery of ofloxacin, *Int. J. Biol. Macromol.*, 84 (2016) 340–348.
- [17] A.B. Albadarin, M.N. Collins, M. Naushad, S. Shirazian, G. Walker, C. Mangwandi, Activated lignin-chitosan extruded blends for efficient adsorption of methylene blue, *Chem. Eng. J.*, 307 (2017) 264–272.

- [18] D. Pathania, D. Gupta, A.H. Al-Muhtaseb, G. Sharma, A. Kumar, M. Naushad, T. Ahamad, S.M. Alshehri, Photocatalytic degradation of highly toxic dyes using chitosan-g-poly(acrylamide)/ZnS in presence of solar irradiation, *J. Photochem. Photobiol., A*, 329 (2016) 61–68.
- [19] G. Sharma, M. Naushad, A. Kumara, S. Rana, S. Sharma, A. Bhatnagar, F.J. Stadler, A.A. Ghfar, M.R. Khan, Efficient removal of coomassie brilliant blue R-250 dye using starch/poly(alginic acid-cl-acrylamide) nanohydrogel, *Process Saf. Environ. Prot.*, 109 (2017) 301–310.
- [20] K. Sharma, V. Kumar, B.S. Kaith, V. Kumar, S. Som, S. Kalia, H.C. Swart, Synthesis, characterization and water retention study of biodegradable Gum ghatti poly(acrylic acid-aniline) hydrogels, *Polym. Degrad. Stab.*, 111 (2015) 20–31.
- [21] G. Sharma, D. Kumar, A. Kumar, A.H. Al-Muhtaseb, D. Pathania, M. Naushad, G.T. Mola, Revolution from monometallic to trimetallic nanoparticle composites, various synthesis methods and their applications: a review, *Mater. Sci. Eng., C*, 71 (2017) 1216–1230.
- [22] J. Zhu, Q. Liu, Z. Li, J. Liu, H. Zhang, R. Li, J. Wang, Recovery of uranium(VI) from aqueous solutions using a modified honeycomb-like porous carbon material, *Dalton Trans.*, 46 (2016) 420–429.
- [23] J.S. Wang, R.T. Peng, J.H. Yang, Y.C. Liu, X.J. Hu, Preparation of ethylenediamine-modified magnetic chitosan complex for adsorption of uranyl ions, *Carbohydr. Polym.*, 84 (2011) 1169–1175.
- [24] E. Piron, A. Domard, Interaction between chitosan and uranyl ions. Part 2. Mechanism of interaction, *Int. J. Biol. Macromol.*, 22 (1998) 33–40.
- [25] H. Li, D. Huang, Microwave preparation and copper ions adsorption properties of crosslinked chitosan/ZSM molecular sieve composites, *J. Appl. Polym. Sci.*, 129 (2013) 86–93.
- [26] A. Mellah, S. Chegrouche, M. Barkat, The removal of uranium(VI) from aqueous solutions onto activated carbon: kinetic and thermodynamic investigations, *J. Colloid Interface Sci.*, 296 (2006) 434–441.
- [27] Q. Liu, J. Zhu, L. Tan, X. Jing, J. Liu, D. Song, H. Zhang, R. Li, Polypyrrole/cobalt ferrite/multiwalled carbon nanotubes as an adsorbent for removing uranium ions from aqueous solutions, *Dalton Trans.*, 45 (2016) 9166–9173.
- [28] M.G. Mahfouz, A.A. Galhoum, N.A. Gomaa, S.S. Abdel-Rehem, A.A. Atia, T. Vincent, E. Guibal, Uranium extraction using magnetic nano-based particles of diethylenetriamine-functionalized chitosan: equilibrium and kinetic studies, *Chem. Eng. J.*, 262 (2015) 198–209.
- [29] I.S. Chaschin, G.A. Badun, M.G. Chernysheva, N.P. Bakuleva, Chitosan adsorption on the collagen tissue of the bovine pericardium from solutions in carbonic acid: role of pressure, *Dokl. Phys. Chem.*, 472 (2017) 32–35.
- [30] J. Li, B. Jiang, Y. Liu, C. Qiu, J. Hu, G. Qian, W. Guo, H.H. Ngo, Preparation and adsorption properties of magnetic chitosan composite adsorbent for Cu<sup>2+</sup> removal, *J. Cleaner Prod.*, 158 (2017) 51–58.
- [31] T. Kamal, Y. Anwar, S.B. Khan, M.T.S. Chani, A.M. Asiri, Dye adsorption and bactericidal properties of TiO<sub>2</sub>/chitosan coating layer, *Carbohydr. Polym.*, 148 (2016) 153–160.
- [32] T.A. Saleh, A. Sari, M. Tuzen, Chitosan-modified vermiculite for As(III) adsorption from aqueous solution: equilibrium, thermodynamic and kinetic studies, *J. Mol. Liq.*, 219 (2016) 937–945.
- [33] M.A. Shaker, A.A. Yakout, Optimization, isotherm, kinetic and thermodynamic studies of Pb(II) ions adsorption onto n-maleated chitosan-immobilized TiO<sub>2</sub> nanoparticles from aqueous media, *Spectrochim. Acta, Part A*, 154 (2016) 145–156.
- [34] R. Huang, Q. Liu, J. Huo, B. Yang, Adsorption of methyl orange onto protonated cross-linked chitosan, *Arabian J. Chem.*, 10 (2013) 24–32.
- [35] D.H. Reddy, S.M. Lee, Application of magnetic chitosan composites for the removal of toxic metal and dyes from aqueous solutions, *Adv. Colloid Interface Sci.*, 202 (2013) 68–93.
- [36] G. Crini, P.M. Badot, Application of chitosan, a natural aminopolysaccharide, for dye removal from aqueous solutions by adsorption processes using batch studies: a review of recent literature, *Prog. Polym. Sci.*, 33 (2008) 399–447.
- [37] F.C. Wu, R.L. Tseng, R.S. Juang, A review and experimental verification of using chitosan and its derivatives as adsorbents for selected heavy metals, *J. Environ. Manage.*, 91 (2010) 798–806.
- [38] R.A.A. Muzzarelli, R. Rocchetti, The use of chitosan columns for the removal of mercury from waters, *J. Chromatogr. A*, 96 (1974) 115–121.
- [39] Y. Chen, J. Wang, Preparation and characterization of magnetic chitosan nanoparticles and its application for Cu(II) removal, *Chem. Eng. J.*, 168 (2011) 286–292.
- [40] L. Zhou, Y. Wang, Z. Liu, Q. Huang, Characteristics of equilibrium, kinetics studies for adsorption of Hg(II), Cu(II), and Ni(II) ions by thiourea-modified magnetic chitosan microspheres, *J. Hazard. Mater.*, 161 (2009) 995–1002.
- [41] D. Hritcu, D. Humelnicu, G. Dodi, M.I. Popa, Magnetic chitosan composite particles: evaluation of thorium and uranyl ion adsorption from aqueous solutions, *Carbohydr. Polym.*, 87 (2012) 1185–1191.
- [42] W. Chen, X. Shen, Y. Hu, K. Xu, Q. Ran, Y. Yu, L. Dai, Z. Yuan, L. Huang, T. Shen, T. Cai, Surface functionalization of titanium implants with chitosan-catechol conjugate for suppression of ROS-induced cells damage and improvement of osteogenesis, *Biomaterials*, 114 (2017) 82–96.
- [43] K.Z. Elwakeel, Removal of reactive black 5 from aqueous solutions using magnetic chitosan resins, *J. Hazard. Mater.*, 167 (2009) 383–392.
- [44] W. Khunawattanakul, S. Puttipatkhachorn, T. Rades, T. Pongjanyakul, Novel chitosan-magnesium aluminum silicate nanocomposite film coatings for modified-release tablets, *Int. J. Pharm.*, 407 (2011) 132–141.
- [45] D.R. Vakilabadi, A.H. Hassani, G. Omrani, B. Ramavandi, Catalytic potential of Cu/Mg/Al-chitosan for ozonation of real landfill leachate, *Process Saf. Environ. Prot.*, 107 (2017) 227–237.
- [46] M.H. Mahaninia, L.D. Wilson, Phosphate uptake studies of cross-linked chitosan bead materials, *J. Colloid Interface Sci.*, 485 (2016) 201–212.
- [47] M. Monier, D.M. Ayad, Y. Wei, A.A. Sarhan, Adsorption of Cu(II), Co(II), and Ni(II) ions by modified magnetic chitosan chelating resin, *J. Hazard. Mater.*, 177 (2010) 962–970.
- [48] P.S. Barber, S.P. Kelley, C.S. Griggs, S. Wallace, R.D. Rogers, Surface modification of ionic liquid-spun chitin fibers for the extraction of uranium from seawater: seeking the strength of chitin and the chemical functionality of chitosan, *Green Chem.*, 16 (2014) 1828–1836.
- [49] C.X. Liu, R.B. Bai, Preparing highly porous chitosan/cellulose acetate blend hollow fibers as adsorptive membranes: effect of polymer concentrations and coagulant compositions, *J. Membr. Sci.*, 279 (2006) 336–346.
- [50] C.X. Liu, R.B. Bai, Preparation of chitosan/cellulose acetate blend hollow fibers for adsorptive performance, *J. Membr. Sci.*, 267 (2005) 68–77.
- [51] C.X. Liu, R.B. Bai, Adsorptive removal of copper ions with highly porous chitosan/cellulose acetate blend hollow fiber membranes, *J. Membr. Sci.*, 284 (2006) 313–322.
- [52] H.İ. Ulusoy, S. Simşek, Removal of uranyl ions in aquatic mediums by using a new material: galloyanine grafted hydrogel, *J. Hazard. Mater.*, 254–255 (2013) 397–405.
- [53] S. Verma, R.K. Dutta, A facile method of synthesizing ammonia modified graphene oxide for efficient removal of uranyl ions from aqueous medium, *RSC Adv.*, 5 (2015) 77192–77203.
- [54] L.C.B. Stopa, M. Yamaura, Uranium removal by chitosan impregnated with magnetite nanoparticles: adsorption and desorption, *Int. J. Nucl. Energy Sci. Technol.*, 5 (2010) 283–289.
- [55] M. Hosoba, K. Oshita, R.K. Katarina, T. Takayanagi, M. Oshima, S. Motomizu, Synthesis of novel chitosan resin possessing histidine moiety and its application to the determination of trace silver by ICP-AES coupled with triple automated-pretreatment system, *Anal. Chim. Acta*, 639 (2009) 51–56.
- [56] M.L. Feng, D. Sarma, X.H. Qi, K.Z. Du, X.Y. Huang, M.G. Kanatzidis, Efficient removal and recovery of uranium by a layered organic-inorganic hybrid thioannate, *J. Am. Chem. Soc.*, 138 (2016) 12578–12585.

[57] W. Liu, X. Zhao, T. Wang, D.Y. Zhao, J.R. Ni, Adsorption of U(VI) by multilayer titanate nanotubes: effects of inorganic cations, carbonate and natural organic matter, Chem. Eng. J., 286 (2016) 427–435.

kinetic model, intraparticle diffusion model, and Elovich model are in the supplementary material. Figures of linearized Freundlich and Langmuir plot, the van't Hoff equation, and the table of thermodynamic parameters are also in the supplementary material.

**Supplementary information**

Figures of N<sub>2</sub> adsorption/desorption isotherm, and the plot of pseudo-first-order kinetic model, pseudo-second-order

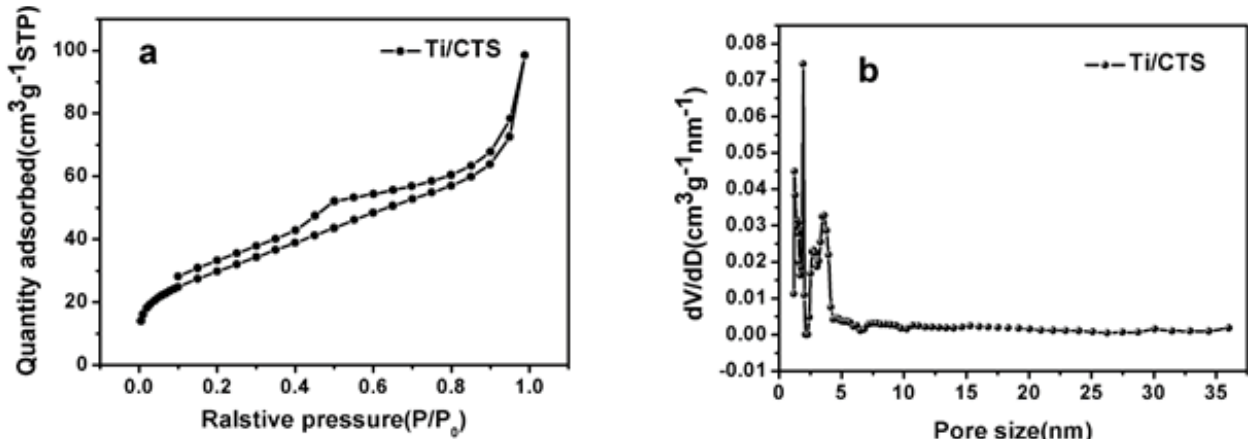


Fig. S1. (a) N<sub>2</sub> adsorption/desorption isotherm and (b) the pore size distributions of Ti/CTS.

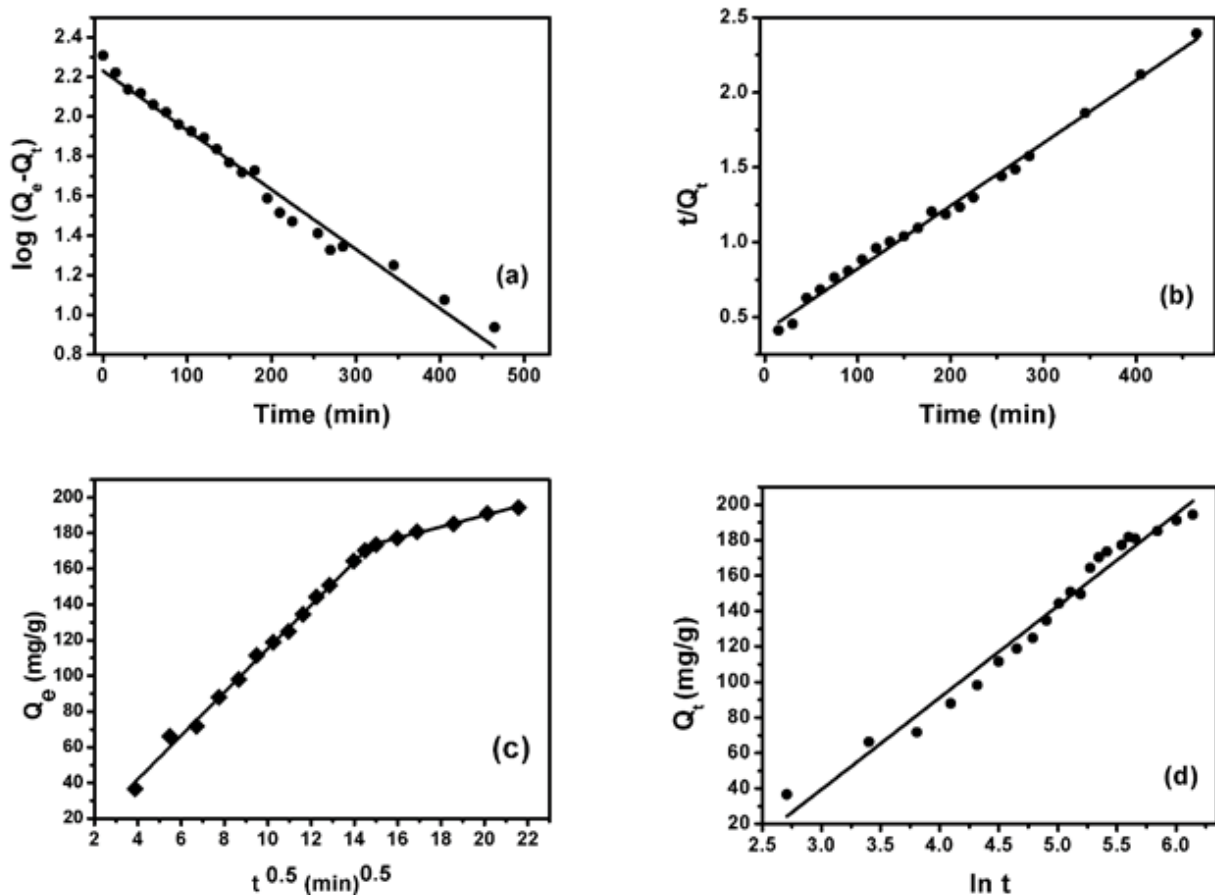


Fig. S2. The adsorption of uranyl ions on Ti/CTS fitted with (a) pseudo-first-order kinetic model, (b) pseudo-second-order kinetic model, (c) intraparticle diffusion model, and (d) Elovich model.

Table S1  
Thermodynamic parameters for  $\text{UO}_2^{2+}$  adsorption onto Ti/CTS

Temperature (K)	$\Delta H^\circ$ (kJ mol <sup>-1</sup> )	$\Delta S^\circ$ (J mol <sup>-1</sup> K <sup>-1</sup> )	$\Delta G^\circ$ (kJ mol <sup>-1</sup> )	$R^2$
298			-6.137	
308	15.823	73.69	-6.874	0.8521
318			-7.610	

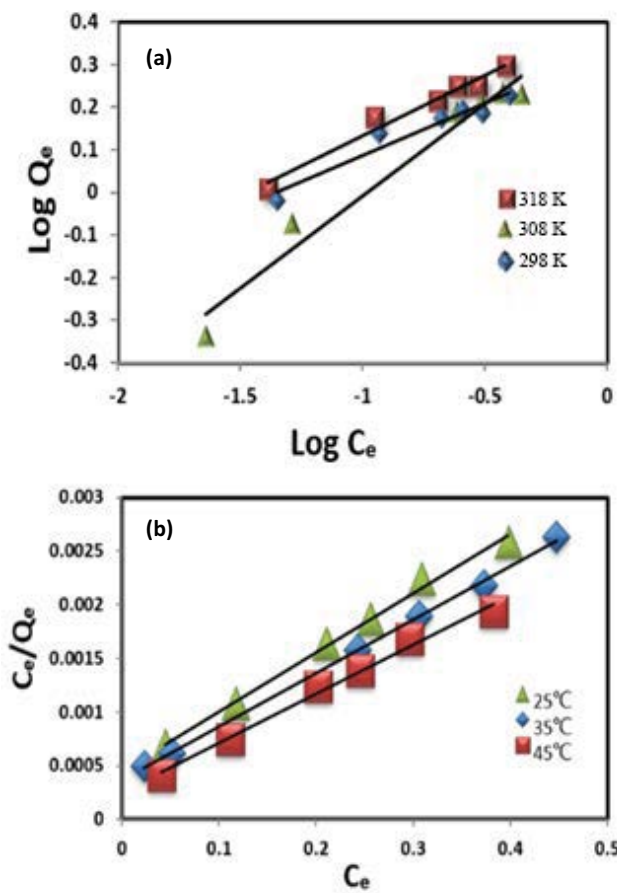


Fig. S3. Adsorption of uranyl ions on ACP as modeled by (a) Freundlich adsorption isotherm and (b) Langmuir adsorption isotherm.

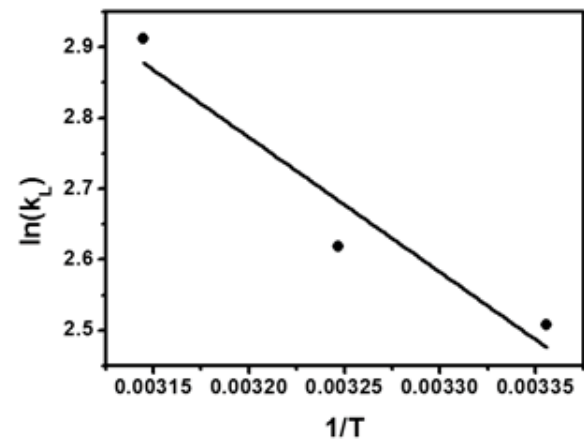


Fig. S4. Linear relationship between  $\ln K_L$  versus  $1/T$  in the van't Hoff equation.